RSC Advances

PAPER

View Article Online
View Journal | View Issue

Cite this: *RSC Adv.*, 2017, **7**, 20888

Restriction of telomerase capping by short non-toxic peptides *via* arresting telomeric G-quadruplex†

Jagannath Jana, Pallabi Sengupta,‡ Soma Mondal‡ and Subhrangsu Chatterjee *

Received 13th December 2016
Accepted 23rd March 2017

DOI: 10.1039/c6ra28149d

rsc.li/rsc-advances

The stabilization of a G-quadruplex structure in human telomeric DNA has become a promising strategy in the development of cancer therapeutics. Here, we report FK13 (a small fragment of human cathelicidin peptide LL37, residues 17–29) and its mutant peptides (KR12A, KR12B and KR12C) inhibiting telomerase activity by stabilizing the telomeric G-quadruplex structures. An array of biophysical studies like fluorescence anisotropy, circular dichroism spectroscopy, circular dichroism melting, isothermal titration calorimetry, and high resolution nuclear magnetic resonance spectroscopy, in conjunction with molecular dynamics simulations, are employed to examine the interaction of peptides with the G-quadruplex structure. Furthermore, the peptide-quadruplex interaction is monitored in *ex vivo* systems, the telomerase over-expressed MCF7 breast adeno-carcinoma cell line. MTT assay and flow cytometry studies indicate selective antiproliferative activities of the peptides towards cancer cells over normal kidney epithelial cell line. Confocal microscopy evidenced nuclear transport and localisation of the peptides. A telomerase repeat amplification protocol assay further evidences telomere uncapping and abrogation of telomerase catalysing activity upon administration of peptides. Hence, arresting G-quadruplex structures using short peptides brings in a new mechanistic insight for the development of future peptide based therapeutics against cancer.

Introduction

Telomeres are composed of nucleoprotein and DNA components at the end of chromosomes.[1] Telomeric DNA consists of G-rich hexanucleotide repeats of DNA sequences (TTAGGG) that fold to adopt non-canonical secondary structures, called G-quadruplexes.[2] G-quadruplex structures play an important role in transcription, recombination and replication.[3] Telomerase,[4] a reverse transcriptase which is over expressed by 85–90% in cancer cells elongates the telomere by adding TTAGGG repeats at the 3′-end and brings in cell proliferation which causes cancer. So inhibition of telomerase activity can be a well approach to tune back the cancer cells to normal cell death. Formation of G-quadruplex at the end of telomeres has been found to inhibit telomerase activity. Therefore, stabilization of G-quadruplexes has become an attractive strategy for the development of anticancer drugs.

Despite great advances in cancer treatment, the emerging multi-drug resistance of cancer cells against conventional anticancer drugs has become life threatening worldwide. The use of conventional chemotherapy is restricted due to toxic side effects. Now in current times designing and developing new drugs with differential skeletons, new modes of action and significantly lower toxicity, especially gene directed therapeutics has become more appropriate and immensely beneficial for mankind. Targeting telomeric DNA G-quadruplex with small molecules as an anticancer therapy has been extensively explored for last few years,[5] but telomeric DNA G-quadruplex targeted by short peptides is yet to be explored. A very few work have been done so far targeting G-quadruplex with peptide. In 2003, Balasubramanian and co-workers describe the generation of novel heterocycle-peptide conjugates that bind to telomeric G-quadruplex DNA.[6] In 2015, Brahim Heddi *et al.* identified an 18-amino acid G-quadruplex-binding domain of RHAU and determined the NMR solution structure of this peptide bound to a parallel DNA G-quadruplex.[7] Several studies showed that various cationic antimicrobial peptides, toxic against bacteria but not to normal mammalian cells, exhibit a broad spectrum of cytotoxic activity against various cancer cell lines.[8] Antimicrobial peptides (AMPs) are normally cationic and amphipathic, carrying a net positive charge ranging from +2 to +9 at the neutral pH.[9] Antimicrobial peptides interact with the lipid membrane of Gram positive and Gram negative bacteria and disrupt their outer membrane.[10,11] Due to higher expression of anionic molecules such as phosphorylserine and *O*-glycosylated mucins cancer cell membrane carries a net negative charge.[12]

Bose Institute, Department of Biophysics, P-1/12 CIT Scheme, Kolkata, 700054, India. E-mail: subhro_c@jcbose.ac.in

† Electronic supplementary information (ESI) available. See DOI: 10.1039/c6ra28149d

‡ These authors contributed equally.

The positively charged peptide (AMPs/anticancer peptides, ACP) strongly binds and disrupts the negatively charged bacterial/cancer cell membranes.[13] Hence, ACPs show selective cytotoxicity against cancer cells compared to that of healthy normal cells. The DNA binding chemotherapeutic drugs perturb DNA synthesis due to non selective binding and hence produce enormous cytotoxicity to normal cells too. A host defense human cathelicidin peptide, LL37, secreted from lung epithelial cells plays an essential role in innate and adaptive immunity.[14] LL37 is an amphipathic peptide with a net positive charge of +6. It shows a broad spectrum of activities against different types of bacteria, fungi, viruses and cancer cells.[15] Previously we reported LL37 efficiently arrests telomeric G-quadruplex structures.[16] Here in this report we show that short and active fragments from LL37 (17–29 residues), FK13 and its mutant peptides inhibit the activity of telomerase *via* targeting and stabilizing the telomeric G-quadruplex structures (Scheme 1).

Materials and methods

Materials

Commercially synthesized oligonucleotide [TAGGG(TTAGGG)3] (GQ23), 5′-TTAGGGTTAGGG-3′ and 5′-CCCTAACCCTAA-3′ (for duplex DNA) were purchased from Eurofins Genomics India Pvt. Ltd. Potassium phosphate monobasic, potassium phosphate dibasic, potassium chloride and *E. coli* 0111:B4 LPS were purchased from Sigma Aldrich. Deuterium oxide (D_2O) and 4,4-dimethyl-4-silapentane-1-sulfonic acid (DSS) was purchased from Cambridge Isotope Laboratories, Inc. (Tewksbury, MA). FITC labelled FK13 was purchased from GL Biochem (Shanghai, China) and all peptides (FK13, KR12A, KR12B and KR12C) were synthesized in Solid phase Peptide synthesizer (Aapptec Endeavor 90) using standard Fmoc chemistry. Synthesized peptides were further purified by reverse phase HPLC system (SHIMADZU, Japan) using Phenomenix C18 column using dual solvent system (water and acetonitrile) containing 0.1% TFA. Molecular weight and purity of the peptides were confirmed using MALDI-TOF. The N-terminal of all the peptides were acelylated and C-terminal were amidated. All experiments were carried out using 10 mM potassium phosphate buffer containing 100 mM potassium chloride at pH 7.0. The oligonucleotide was dissolved in the above mentioned buffer and heated in water bath at 95 °C for 10 minutes. The oligonucleotide was slowly cooled to room temperature and then stored at 4 °C for 24 hours.

Methods

Fluorescence spectroscopy. All fluorescence experiments were carried out using Hitachi spectrophotometer (F-700 FL spectrophotometer). Fluorescence spectra were measured using

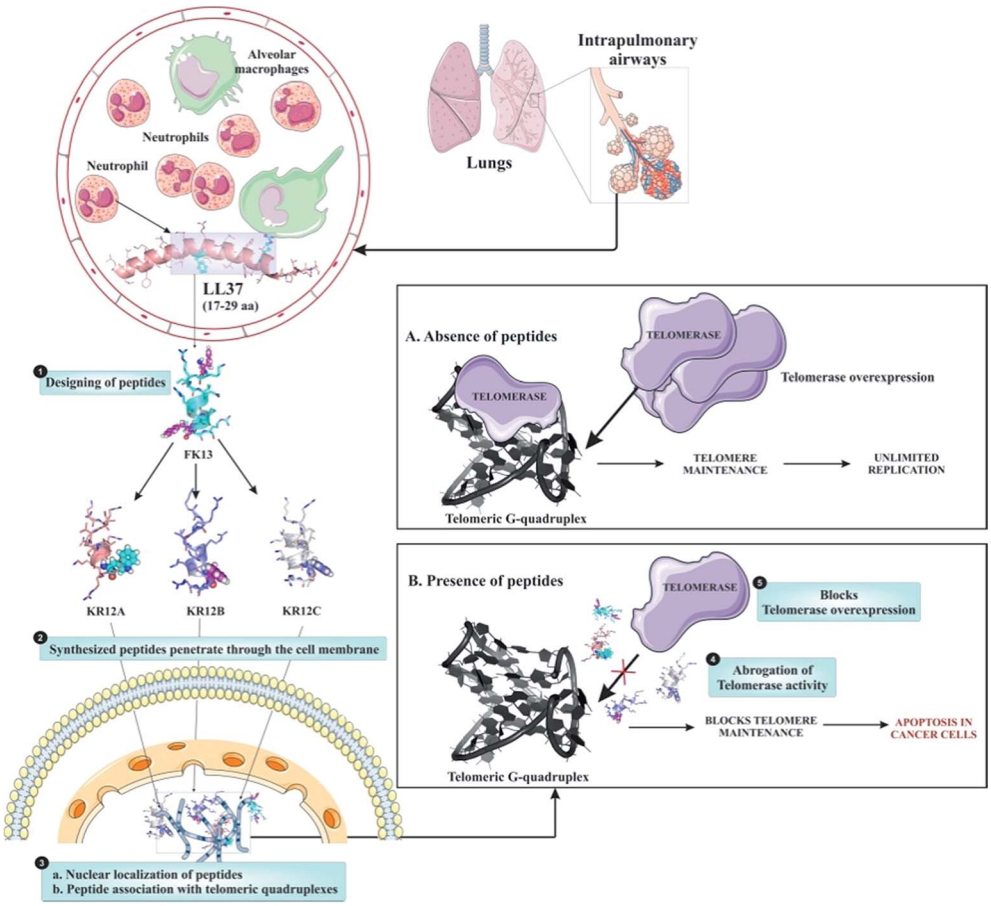

Scheme 1 Proposed mechanism of action of short peptides binding to telomeric G-quadruplex.

0.1 cm cuvette. Excitation and emission slit were 5 nm. The binding of GQ23 and FK13 were measured from 300–500 nm with excitation wavelength of 260 nm. Steady-state anisotropy was recorded with Hitachi model F-700 FL spectrometer equipped with a polarized accessory. The fluorescence anisotropy (r) values were obtained using the expression equation:

$$r = (I_{VV} - GI_{VH})/(I_{VV} + 2GI_{VH})$$

$$G = I_{HV}/I_{HH}$$

where I_{VV} and I_{VH} are emission intensities of the parallel and perpendicularly polarized light at 348 nm respectively. G is correction factor. The slits for excitation and emission were set at 5 nm. 10 μM peptides (KR12A, KR12B and KR12C) were titrated with increasing concentrations of GQ23. The anisotropy data were fitted using the following ligand binding equation:

$$r = B_{max}L(K_D + L)^{-1}$$

where r= fluorescence anisotropy, L = quadruplex concentration and K_D = dissociation constant.

Circular dichroism spectroscopy. CD spectra were measured using Jasco 815 spectrometer. Spectra were obtained with accumulation of three scans, at a speed of 100 nm min^{-1}, scanned over a range of 210–320 nm and 200–260 nm for GQ23 and peptides, respectively with data interval of 1 nm. Cuvette of path length 0.1 cm was used. 20 μM of GQ23 was titrated with increasing concentration (20–60 μM) of peptides. 20 μM peptides were titrated with increasing concentration (20–60 μM) of LPS. CD melting studies were performed with free GQ23, GQ23 : peptide (1 : 3), free duplex and duplex-FK13 complex (1 : 3) from 10–90 °C temperature range separately. The delay time was 150 second. Temperature interval and Ramp rate were 5 °C and 2.5 °C min^{-1}, respectively.

Isothermal titration calorimetry. The ITC experiments were performed using a VP ITC Micro calorimeter at 25 °C. A samples cell containing 10 μM peptides were titrated against 300 μM quadruplex GQ23. Samples were extensively degassed prior to titration. Total no. of injection was 20 at an interval of 150 seconds with 2 μL quadruplex per injection. The raw data were analyzed using Origin software provided with the instrument. The data were fitted using one set of site model. Equilibrium association constant (K_A), change in enthalpy of reaction (ΔH), change in Gibb's free energy (ΔG) and entropy (ΔS) were calculated using the following equation:

$$\Delta G = \Delta H - T\Delta S$$

To determine the binding affinity of peptides with duplex DNA, 10 μM peptides were titrated with 300 μM duplex DNA keeping other parameters identical with that of peptides-GQ23 binding. The data points obtained were fitted into 'three set of sites' binding model.

Nuclear magnetic resonance spectroscopy. All NMR spectra were recorded using Bruker AVANCE III 500 MHz NMR spectrometer equipped with a 5 mm SMART probe at 298 K. Data processing and acquisitions were performed with Topspin™ v3.1 software. Two-dimensional total correlation spectroscopy (TOCSY) and nuclear overhauser effect spectroscopy (NOESY) spectra of free peptides (1 mM) and peptide in LPS were acquired in aqueous solution containing 10% D_2O at pH 4.5. The mixing time for TOCSY and NOESY were 80 and 150 ms respectively. Two dimensional trNOESY experiments were performed using 1 mM peptides by titrating various concentrations of LPS ranging from 5 to 25 μM. DSS (2,2-dimethyl-2-silapentane 5-sulfonate sodium salt) was used as an internal standard (0.0 ppm). A series of one dimensional proton and proton decoupled ^{31}P NMR experiment were performed using the Bruker pulse programme "zgesgp" and "zgpg30" respectively.

Calculation of NMR derived structures. All the NMR structures of peptides were calculated using CYANA program v2.1. NOE intensities were qualitatively categorized as strong, medium, and weak based upon their respective cross-peak intensities from trNOESY spectra obtained in presence of LPS. This inter proton upper-bound distances were 3.0, 4.0 and 5.0 Å respectively. The lower bound distance was reserved constant at 2.0 Å. To restrict the conformational space for all residues, the backbone dihedral angle (phi) was varied from −30° to −120°. No hydrogen bonding constrains were used for structure calculation. Several round of structure refinements were performed and based upon the NOE violations, the distance restraints were adjusted accordingly. The ten lowest energy structures were selected to generate ensembles of structures of peptides bound to LPS. The structures were analyzed using pymol.

Molecular dynamics simulation. MD simulations were performed in Amber14 using prmbsc0 modifications with ff99SB force field for GQ23 and GQ23-FK13 complex.[17,18] Two K^+ ions were added in the central core of GQ23. The K^+ ions were also added to counter stabilized the solvated system. To solvate the system in an octahedral model TIP3P water model were used with edge length extensions of 10 Å from solute atom.[19] The particle mesh Edward simulation method was employed to perform the simulation using periodic boundary conditions.[20] To correct long range van der Waals interactions, Lennard-Jones potentials and direct space interactions cutoff were 9 Å. SHAKE algorithm were used for restraining hydrogen atoms with integration time step of 2 fs.[21] The energy minimization was done in explicit solvent conditions. MD simulations were continued upto 50 ns. The trajectory was collected at an interval of 2 ps for all system. The trajectory of MD simulation were analyzed using cpptraj module of Amber tools14.[22]

Cell culture. MCF7 (human breast adenocarcinoma cell line) (NCCS, Pune) and NKE (normal kidney epithelial) cells (gifted from Dr Kaushik Biswas, Bose Institute) were maintained in complete DMEM (Himedia; AL007G) and RPMI 1640 media (Himedia; AL120A) respectively, supplemented with 10% FBS (fetal bovine serum), 2 mM L-glutamine, 500 μL of 50 mg mL^{-1} gentamycin, 1 mL Pen-Strep, and 750 μL amphotericin B in a fully humidified incubator (ESCO cell culture CO_2 Incubator, model no. CCL-1708-8-UV) at 37 °C and 5% CO_2.

MTT assay. MCF7 cells were grown in DMEM medium supplemented with 10% FBS, penicillin (100 μg mL^{-1}) and streptomycin (100 μg mL^{-1}). Cells were seeded into 96-well culture

plates at a density of 8000 cells/well and cultured overnight at 37 °C and 5% CO_2. The cells were then treated with varying concentrations of peptides (20 μM, 40 μM, 60 μM and 80 μM) in triplicate condition and incubated for 24 hours. The MTT dye (concentration of 0.5 mg mL^{-1}) was added after 24 hours and again incubated at 37 °C for 4 hours. The optical density of each well was then read at 570 nm using a Biotek ELx800 microplate reader. The percent of cell viability of treated cells was calculated by the following equation:

$$(A_{\text{tested}} - A_{\text{media control}})/(A_{\text{drug-free control}} - A_{\text{media control}}) \times 100\%$$

where A is the mean value calculated by using the data from three replicate tests.

Flow cytometry. MCF7 cells were seeded into 6 well microtiter plates at a density of 1×10^6 cells per well. Cells were treated with FK13, KR12A, KR12B, and KR12C at increasing concentration gradient for 24 hours. The flow cytometric assay was carried out with BD Pharmigen™ Annexin V-FITC Apoptosis detection Kit (Catalog no. 556570) as per manufacturer's protocol. In brief, cells were trypsinized and washed twice with 1× PBS followed by resuspension in 1× binding buffer (Catalog no. 556454). Thereafter, 5 μL of Annexin V-FITC (Catalog no. 556420) and 2 μL of PI (Catalog no. 556463) were added, protected from light, and incubated for 30 min and 15 min respectively. Finally, the cell suspensions were diluted into 1× binding buffer immediately prior to flow cytometric analyses in BD FACS Verse™ Flow cytometer. All the measurements were carried out with three replicates with data acquisition at 1000 number of events and medium flow rate. 60 μM Etoposide treated cells were considered as positive controls.

Cell cycle arrest assay. MCF7 cells were sub-cultured into 6 well microtiter plates at a density of 1×10^6 cells per well. Cells were treated with FK13, KR12A, KR12B and KR12C respectively from 0 to 40 μM concentrations for 24 hours. Cells were harvested by trypsinization and washed with cold 1× PBS. Then, cells were fixed with chilled 80% ethanol and stored at −20 °C overnight. After fixation, cells were resuspended into cold 1× PBS, containing 10 μg mL^{-1} RNase A (Sigma) and incubated at 37 °C for 2 hours. Then PI (propidium iodide) (Sigma) was added at a final concentration of 1 μg mL^{-1} and incubated in 4 °C, dark, at mild rocking condition. Cells were analyzed for DNA content using BD FACS Verse™ FACS flow cytometer.

Confocal microscopy. Cellular localization of the peptide was monitored by confocal microscopy. Around 2.5×10^6 number of MCF7 cells were cultured on 35 mm diameter glass-bottomed cover slips for 24 h followed by incubation with FITC-FK13 (20 μM) for 0–24 hour inside CO_2 (5%) incubator at 37 °C. After 0–24 hour incubation, cells were washed with PBS for three times to remove excess FITC-FK13. The cells were fixed with 3.7% pre warmed formaldehyde (37 °C) for 15 minutes. Again the cells were washed with PBS for three times. The cells were then stained with DAPI (3 μL in 1 mL PBS from 2 mg mL^{-1} stock in DMF) and incubate for 15 minutes in dark. Then the cells were washed with PBS for three times to remove excess DAPI.

RT-PCR. Total RNA was isolated from cultured MCF7 cells using TRIzol method (Invitrogen, Carlsbad, CA) as per manufacturer's instructions. 2 μg of total RNA was processed for cDNA synthesis and reverse transcribed (RT) by Super MuLV RT Kit (Biobharati Life Sciences Pvt. Ltd.). PCR reactions were optimized to 94 °C for 2 min, 35 amplification cycles at 94 °C for 30 s, the appropriate annealing temperature for 30 s, 72 °C for 45 s, and a final extension of 5 min at 72 °C. The final products were electrophoresed on 1.5% agarose gels and visualized by ethidium bromide staining along with DNA markers. Reactions were carried out in triplicates and housekeeping gene GAPDH was used as internal control to normalize the variability in expression levels. PCR primers were designed using Primer BLAST, NCBI and analysed in OligoAnalyser 3.1-IDT. The forward and reverse primer sequences and corresponding annealing temperatures are listed in Table 1.

Telomerase repeat amplification protocol assay. TRAP assay was performed using MCF7 breast cancer cell line. The Quantitative Telomerase Detection Kit was purchased from Allied Biotech Products (MT3011). TRAP assay was performed with 0, 2 and 5 μM peptides while keeping the total reaction volume at 25 μL. Each experiment was performed in triplicates. The transform fold change in telomerase activity was calculated and the experimental condition was maintained as reported previously.[23]

Statistical analyses. The statistical significance is determined by Student's t test. The results are averaged from three independent experiments. Error bars demonstrate mean ± standard deviation. $P < 0.05$ is considered to be statistically significant.

Results and discussion

Designing of peptides

LL37, an antimicrobial and anticancer peptide, attains α-helical conformation in presence of negatively charged lipid environment.[24] It directly interacts with negatively charged bacterial and cancer cell membrane *via* electrostatic attraction. Previously we have shown that LL37 binds to telomeric G-quadruplex. However, it is difficult to develop LL37 as a therapeutic agent because of its large size. Thus our aim is to develop short and active peptide from LL37 for lower cost of production and better selectivity. Xia Li *et al.* showed a 13 residue peptide (FK13), corresponding to 17–29 residues of LL37, exhibits antimicrobial and anticancer activity, though the mechanism of its action is not fully explored.[24] In addition, residues 18–29 of LL-37 (KR12) are identified as the smallest region possessing antimicrobial activity.[25] In 2013, Song Yub Shin designed and synthesized a series of amino acid-substituted analogs from the α-helical wheel diagram of KR-12 to optimize short α-helical AMPs having both antimicrobial and antiendotoxic activities without mammalian cell toxicity.[26] Among the analogs of KR12, these peptides (KR12A, KR12B and KR12C) showed much higher cell specificity for bacteria compare to parental LL-37. AMPs containing Trp shows potent antimicrobial activity compared to Tyr or Phe.[27] In this context, we have taken FK13 and short analogs of KR12 (Table 2) by substitution of several amino acids which can inhibit the activity of enzyme telomerase by arresting telomeric G-quadruplex structure.

Table 1 The forward and reverse primer sequences and corresponding annealing temperatures

Gene	RTPCR primer sequences (5′–3′)	Annealing temperature (°C)
hTERT	F-GCAAGTTGCAAAGCATTGGAATCAGACAGC (30 bp)	58
	R-CTCGTAGTTGAGCACGCTGAACAGTG (26 bp)	58
GAPDH	F-GATGCTGGCGCTGAGTACGTCGTG (24 bp)	62.5
	R-AGTGATGGCATGGACTGTGGTCATGAG (24 bp)	62.5

Table 2 Amino acid sequences of peptides used for the study

Peptides	Sequences	Net charge
FK13	FKRIVQRIKDFLR	+5
KR12A	KRIVQRIK**KW**LR	+7
KR12B	KRIV**K**RIK**KW**LR	+8
KR12C	KRIV**KL**IK**KW**LR	+7

Binding of peptides (FK13, KR12A, KR12B and KR12C) to human telomeric G-quadruplex by fluorescence spectroscopy

The association of peptides (FK13, KR12A, KR12B and KR12C) with telomeric G-quadruplex (GQ23) are monitored using fluorescence spectroscopy. The quantum yield of Phe is five times less compared to Trp. Hence we monitor blue shift in the emission spectra of GQ23 bound to FK13. On the other hand, KR12A, KR12B and KR12C containing Trp show emission maxima near 340 to 348 nm whereas G-quadruplex displays emission near 340 nm. To avoid complexities we have performed fluorescence anisotropy of KR12A, KR12B and KR12C in presence of increasing concentration of GQ23. GQ23 exhibits emission maxima at 338 nm in phosphate buffer solution. Upon addition of FK13 into GQ23 at an increasing concentrations show a significant blue shift in the emission maxima (Fig. S1†). Total blue shift after complete binding of FK13 to GQ23 is found to be 10 nm. A plot of $\Delta\lambda$ (FK13 bound-free) of fluorescence emission *vs.* FK13 concentration provides the binding curve (Fig. S2A†). The blue shift in the emission spectra indicates that FK13 binds to GQ23. On the other hand, the binding of peptides (KR12A, KR12B and KR12C) with GQ23 is observed by an increase in fluorescence anisotropy. An increase in fluorescence anisotropy of peptides (KR12A, KR12B and KR12C) upon increasing concentrations of GQ23 indicates association of peptides with GQ23 (Fig. S2B–D†). Binding of peptides (KR12A, KR12B and KR12C) to GQ23 reduces its mobility resulting in an increase of anisotropy of peptides in the bound form. The dissociation constant of the peptides binding to GQ23 ranges from 3–24 μM (Fig. S2†).

CD spectroscopy reveals the interaction of peptides (FK13, KR12A, KR12B and KR12C) with human telomeric G-quadruplex

CD spectroscopy is performed to unravel the structural changes of G-quadruplex upon interaction with peptides (FK13, KR12A, KR12B and KR12C). Parallel G-quadruplex shows a positive peak near 260 nm with a negative minima near 240 nm whereas antiparallel G-quadruplex shows a positive peak at 290 nm and a negative peak at around 260 nm. Hybrid G-quadruplex structure is characterized by the existence of a major positive peak at 290 nm, a hump at 270 nm and a minor negative peak at 235 nm in presence of potassium ions.[28] GQ23 folds to adopt hybrid conformation as indicated by the presence of a positive peak at 290 nm, a hump at 268 nm and a negative peak at 236 nm. Upon addition of FK13 into GQ23 at a ratio of 1 : 3 showed almost no change of the hybrid conformation of GQ23 (Fig. S3A†). However, successive addition of KR12A, KR12B and KR12C into GQ23 upto a ratio of 1 : 3 showed a decrease in ellipticity at 290 nm and 268 nm (Fig. S3B and C†). The decrease in ellipticity at 290 nm and 268 nm is attributed due to binding of the peptides to GQ23.

CD melting determines structural stability of peptide-G-quadruplex complex

CD melting experiments are employed to observe the structural stability of peptides-G-quadruplex complexes. The stability of GQ23 increases in the presence of peptides (FK13, KR12A, KR12B and KR12C) in comparison with its free state. The CD melting temperature (T_m) of free GQ23 is found to be 62 °C. The CD melting of free GQ23 show that the folded hybrid conformation of GQ23 is almost lost within 65 °C to 70 °C (Fig. S4†). Interestingly, we have observed a structural transition from hybrid conformation to parallel conformation at higher temperature (above 65 °C) for all G-quadruplex-peptide complexes (1 : 3) (Fig. 1). In addition, the population of parallel conformation of GQ23 bound to peptides (at the ratio 1 : 3) decreases from 65 °C to 90 °C. The CD melting of duplex DNA–peptides complex (1 : 3) is also performed to evaluate the binding specificity of peptides towards duplex DNA. The CD melting temperature (T_m) of free duplex DNA and duplex DNA-peptides complex are found to be 44.4 °C and 47.3 °C (FK13), 52.9 °C (KR12A), 53 °C(KR12B), 51.8 °C (KR12C) respectively (Fig. S5†). This result demonstrates that the peptides provide higher selectivity to telomeric G-quadruplex compared to duplex DNA.

Thermodynamics of binding of peptide-G-quadruplex complex by isothermal titration calorimetry

Isothermal Titration Calorimetry (ITC) is performed to get the detailed insight into the thermodynamic parameters of binding of peptides to G-quadruplex. The equilibrium binding constant (K_D) and the changes in thermodynamic parameters such as enthalpy (ΔH), Gibbs free energy (ΔG) and entropy (ΔS) are obtained by ITC for all peptides (FK13, KR12A, KR12B and KR12C) binding to GQ23. The thermodynamic parameters and the thermograms obtained for the association of four peptides

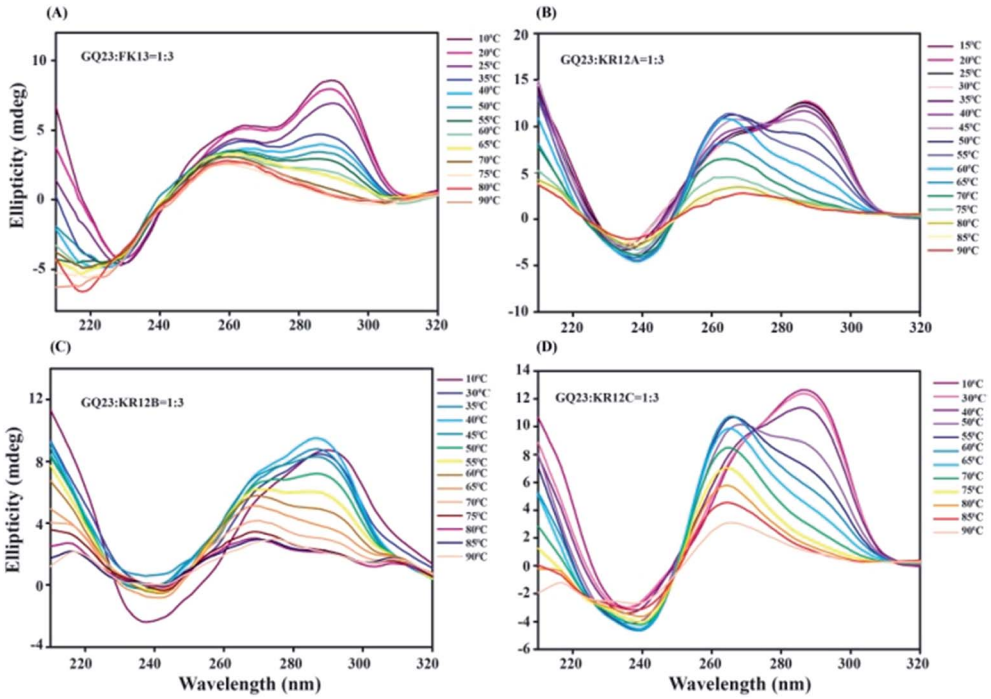

Fig. 1 CD melting profile of GQ23-peptide complex (1 : 3) showed structural transition from hybrid conformation to parallel conformation at higher temperature (~65 °C). GQ23-FK13 complex (A), GQ23-KR12A complex (B), GQ23-KR12B complex (C) and GQ23-KR12C (D). The concentration of GQ23 and peptides were 20 μM and 60 μM respectively.

with GQ23 are listed in Table 3 and Fig. 2A–D respectively. The thermograms depict one set of binding event for all peptides binding to GQ23. The negative values of enthalpy (ΔH) and entropy (ΔS) substantiate the formation of hydrogen bonds and van der Waal interactions between the *G* quadruplex and peptides. An overall negative free energy of binding ($\Delta G < 0$) indicates that the binding of GQ23 with all the four peptides (FK13, KR12A, KR12B and KR12C) are spontaneous in nature. Table 3 shows that the binding affinity of KR12C towards GQ23 is stronger as compared to FK13, KR12A and KR12B (FK13 < KR12A < KR12B < KR12C). The association of peptides with duplex DNA shows that the peptides have a higher binding affinity (1.5 to 10 fold) for quadruplex (GQ23) than the corresponding duplex DNA (Fig. S6 and Table S1†).

Atomic level interaction of FK13 with human telomeric G-quadruplex by NMR spectroscopy

The high resolution NMR experiments are performed to characterize the interaction between GQ23 and FK13 and enlighten the structure of the complex. One dimensional imino proton spectra of free GQ23 is a signature of the quartet formations. Fig. S7† showed an array of one dimensional imino proton spectrum of GQ23 with increasing concentrations of FK13 up to 1 : 3 (GQ23 : FK13) ratio. In absence of FK13, GQ23 exists in a monomeric, globular and folded conformation as indicated from the sharp imino signals of 9-guaninyl residues. Progressive addition of FK13 to this folded conformation (up to a final molar ratio of GQ23 : FK13 = 1 : 3) shows chemical shift perturbation as well as line broadening in imino signals in ^{1}H spectra of GQ23, indicating G-quartet-FK13 interaction. One dimensional proton decoupled ^{31}P NMR experiments are carried out to show the interaction between the phosphate backbone of GQ23 and FK13. Fig. S8† shows an array of one dimensional ^{1}H decoupled ^{31}P NMR spectrum of GQ23 and its complex with increasing concentrations of FK13 up to a molar ratio of 1 : 3 (GQ23 : FK13). One dimensional ^{31}P NMR spectra of GQ23 shows significant line broadening upon addition of FK13 indicating strong interaction between phosphate backbone of GQ23 and FK13.

Table 3 Thermodynamic parameters obtained from ITC experiment

Parameters	FK13	KR12A	KR12B	KR12C
K_A (M^{-1})	1.61×10^4	3.31×10^4	4.72×10^4	5.71×10^4
K_D (μM)	62.11	30.21	21.18	17.51
ΔH (cal mol^{-1})	-5.43×10^4	-2.86×10^4	-5.047×10^4	-6.28×10^4
ΔS (cal mol^{-1} K^{-1})	−163	−75.3	−148	−189
ΔG (Kcal mol^{-1})	−5.72	−6.16	−6.37	−6.48
Binding stiochiometry (*n*)	1.15 ± 0	1.15 ± 0.70	1.4 ± 0.30	1.17 ± 0.21

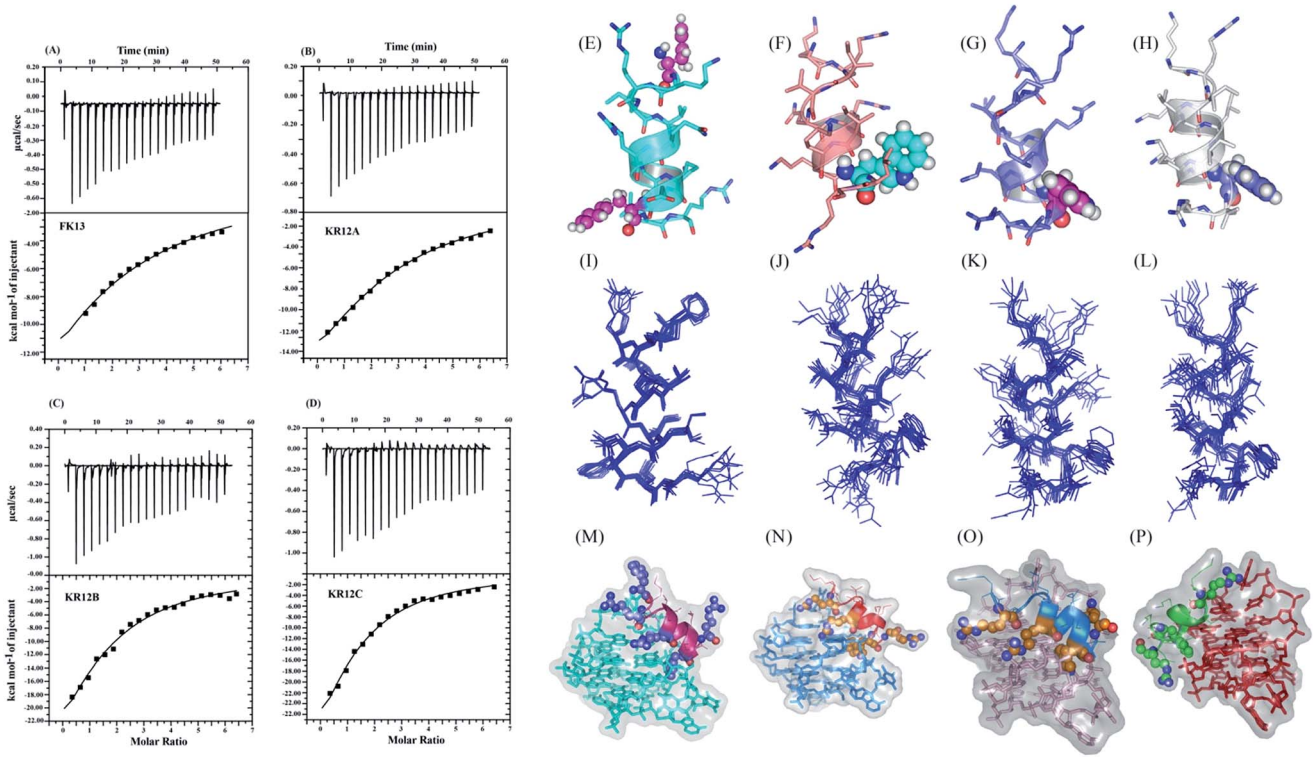

Fig. 2 Isothermal Titration Calorimetry (ITC) profile of peptides binding to GQ23. FK13-GQ23 binding (A), KR12A-GQ23 binding (B), KR12B-GQ23 binding (C) and KR12C-GQ23 binding (D). The solid line represents the best fit data using 'one site binding model'. NMR derived three dimensional structures of FK13 (E), KR12A (F), KR12B (G) and KR12C (H) in LPS micelle. Superimposition of 10 lowest energy conformers of FK13 (I), KR12A (J), KR12B (K) and KR12C (L). Docked structures of GQ23 with peptides FK13 (M), KR12A (N), KR12B (O) and KR12C (P).

Three dimensional structures of peptides (FK13, KR12A, KR12B and KR12C) bound to LPS micelle

Lipopolysaccharide (LPS) is a glycolipid component present in the outer membrane of Gram negative bacteria forms negatively charged micelle at very low concentration. AMPs carrying positive charge can strongly interact with LPS through electrostatic attraction. However, most of the cancer cell membrane carries a net negative charge because of higher expression of anionic molecules such as phosphorylserine and *O*-glycosylated mucins. Several reports suggest the strong electrostatic interaction between cationic anticancer peptides and negatively charged cancer cells.[29] Taken together, we take LPS as a model system to determine the structures of these peptides in negatively charged cancer cells. LPS forms a high molecular weight micelles even at a very low concentration (<1 μM).[30] The secondary structures of the peptides FK13, KR12A, KR12B and KR12C are determined using CD spectroscopy. Fig. S9† shows far UV-CD spectra of the peptides in presence and absence of LPS. In aqueous solution, all the peptides show negative peak at 200 nm indicating random coil structures. The entire peptides show two negative peaks, one at 208 nm and other at 222 nm in presence of LPS demonstrating their α-helical conformation.

To gain the detailed structural information of the peptides we have determined their three dimensional structures in presence of LPS using transferred Nuclear Overhauser Effect Spectroscopy (trNOESY) experiments.[31] The complete sequence specific proton resonance assignments were determined using both two-dimensional total correlation spectroscopy (TOCSY) and NOESY. The NOESY spectra for all the peptides showed only a weak intra- and sequential NOE between the backbone and side chain proton resonances (data not shown). On the other hand, addition of LPS even in small quantity to FK13, KR12A, KR12B and KR12C show a marked increase in the number of NOEs, owing to the fact that peptide adopts a folded conformation in presence of LPS (Fig. S10†). The sequential $\alpha N(i, i+1)$ trNOEs and a large no of medium range $\alpha N(i, i+3/i+4)$ NOEs are obtained in presence of LPS (Table S4†). The three dimensional structures of the peptides are determined on the basis of distance restraints obtained from the trNOESY experiments. All the four peptides adopt α-helical conformation in presence of LPS (Fig. 2H and I). Fig. 2I–L shows superimposition for an ensemble of 10 lowest energy structures of FK13, KR12A, KR12B and KR12C respectively.

The possible GQ23-peptides complex formation and atomic level interaction by docking and molecular dynamics simulation

The feasible complex formation between G-quadruplex and peptides are obtained by docking in ZDOCK version 3.0.2 [GQ23 were obtained from PDB (PDB ID: 2JSM)].[32] The NMR structures of the peptides are found to be docked on the 3′-end of GQ23. The side chain of Arg7 of FK13 holds the phosphate

backbone of GQ23 (Fig. 2M). The side chains of Arg2 and Arg6 bind to (forming hydrogen bond) the phosphate backbone of GQ23 for KR12A (Fig. 2N). The positively charge side chains of Arg6 and Arg12 interact with negatively charged phosphate backbone of GQ23 for KR12B (Fig. 2O). The side chains of Arg2 and Arg12 form hydrogen bond with phosphate and T13 respectively for KR12C (Fig. 2P). Further, to get the detailed insight to the mechanism of binding, molecular dynamics simulation is performed for 50 ns for GQ23–FK13 complex. From MD simulation studies we have seen that Arg3, Arg7 and Arg13 hold the phosphate backbone of GQ23 (Fig. S11B†). The peptide FK13 lost its helicity after 40 ns MD simulation (Fig. S11B†). The RMSD of GQ23-FK13 complex is found to be less compared to its free GQ23 demonstrating FK13 stabilizes GQ23 (Fig. S12†).

The peptides (FK13, KR12A, KR12B, and KR12C) selectively induce cytotoxicity in telomerase overexpressing cancer cells

Previous studies have shown that MCF7 cells exhibit elevated telomerase activity than the normal kidney epithelial cells.[33,34] Therefore, to examine the cytotoxic effects of the peptides, we have treated MCF7 (human breast adenocarcinoma cell line) and NKE (normal kidney epithelial) cell lines with FK13, KR12A, KR12B and KR12C at increasing concentration gradient (0–80 μM) for 24 hours, and monitored cell proliferation by MTT assay. Results indicate a marked and dose-dependent reduction in cell proliferation after 24 hours of treatment (Fig. 3A–D, Table S2†). Among these four peptides, FK13, KR12A, and KR12B induce meager cytotoxicity to MCF7 cells at 40 μM (cell viability-75%, 77%, and 84% respectively) and 60 μM (cell viability-70%, 72%, and 64%, respectively) concentration. However, an escalation to 80 μM concentrations does not implement even 50% depletion in cell viability. On the contrary, KR12C having the IC_{50} value of 43 ± 1.5 μM exerts maximum cytotoxicity compared to other tested peptides (cell viability-53% at 40 μM and 46% at 60 μM respectively). On the other hand, NKE cells, which are predisposed with lower telomerase activity, are appreciably unaffected from the cytotoxic insults of the peptides (Fig. 3E–H and Table S3†).

The peptides (FK13, KR12A, KR12B, and KR12C) stimulates pro-apoptotic signal to telomerase overexpressing cancer cells

Based on the above results of MTT assay, we have carried out flow cytometry-based apoptosis detection experiments in MCF7 cells to speculate the mode of growth inhibition by these peptides. In this experiment, MCF7 cells are treated with these four peptides in a concentration dependent manner for 24 hours and subjected to Annexin V/PI staining for the quantitative assessment of live, early and late apoptotic, and necrotic or dead populations. The results demonstrate that FK13 and KR12A do not alter cell survivability at 20 and 40 μM as more than 80% cells remain live in this concentration range. The percentage of the early apoptotic population in FK13 treated cells are 4.44%, and 4.05% and in KR12A treated cells are 3.61%, and 5.08% at 20 and 40 μM respectively which scores these two peptides as weak apoptosis inducers (Fig. 4). Further raise in their concentration to 60–80 μM range, fail to achieve the IC_{50} value (concentration at which 50% cells are alive) in either case. However, KR12B and KR12C are competently inducing death signal in cancer cells. Percentage of the apoptotic population in KR12B (40 μM) treated MCF7 cells is 74.91% (early + late apoptotic) which is significantly higher than those of FK13 and KR12A. This result clearly indicates that KR12B can induce apoptosis more significantly. Similarly, in KR12C treated set, at 40–80 μM, the apoptotic population gradually increases (22.73% at 60 μM and 26.86% at 80 μM respectively) which underlies its greater potency in declining cell viability. Hence the flow cytometric results are consistent with MTT assay as the anti-proliferative and anti-cancer attributes of KR12B and KR12C are found to be more pronounced than the rest of the tested peptides in both the cases.

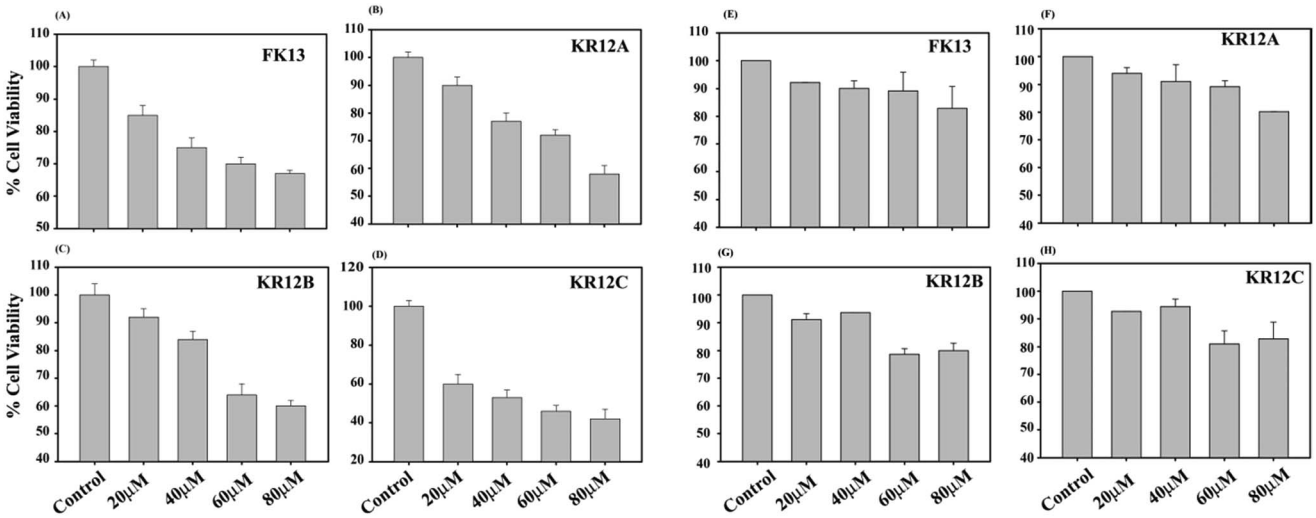

Fig. 3 Percentage of cell viability of MCF7 cells treated with peptides, FK13 (A), KR12A (B), KR12B (C) and KR12C (D) after 24 hours incubation. Percentage of cell viability of NKE cells treated with peptides, FK13 (E), KR12A (F), KR12B (G) and KR12C (H) after 24 hours incubation.

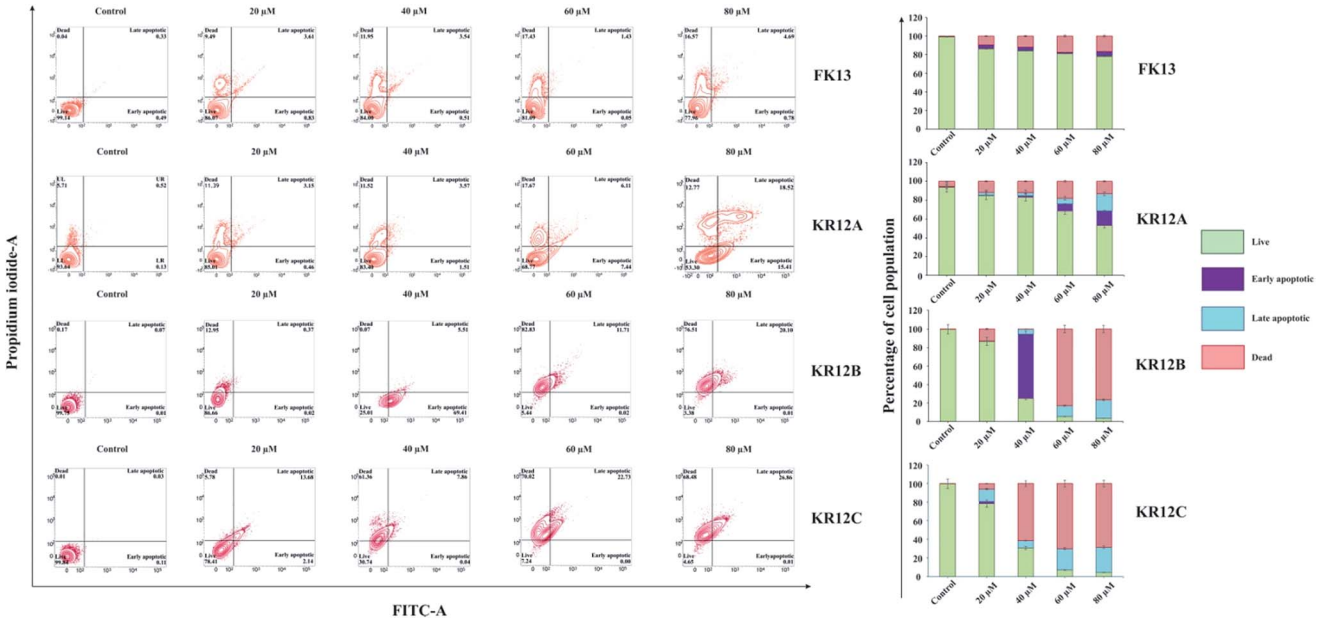

Fig. 4 Flow cytometric analysis of apoptosis in MCF7 and NKE cell lines treated with increasing concentration of synthetic short peptides for 24 hours. All the peptides are able to induce apoptosis in cancer cells. KR12B and KR12C are more competently promoting apoptosis than FK13 and KR12A. An etoposide treated positive control was considered (data not shown). Percentage of live, early apoptotic, late apoptotic and necrotic cell population were represented in stackedbar plot.

The peptides (FK13, KR12A, KR12B, and KR12C) perturb cell cycle progression at G2/M transition

We have explored another aspect of anti-proliferation by these peptides through the determination of cell cycle distribution in MCF7 cells. In this study, MCF7 cells are treated with various concentrations of the peptides for 24 hours and cell cycle perturbation is quantitatively analysed by flow cytometry. With increasing peptide concentrations (0–40 μM), a prominent hike in Sub G0 population is evidenced which corresponds to the apoptotic population (Fig. S13†). At 20 μM, the Sub-G0 population in KR12B and KR12C treated sets notably increase by 45.12% and 26.1% respectively than the elevation in FK13 and KR12A-treated ones (3.08% and 14% respectively). This result is corroborating with the earlier Annexin V-FITC/PI binding assay which suggests KR12B and KR12C as strong apoptosis inducers as compared to FK13 and KR12A. Moreover, MCF7 cells treated with FK13, KR12A, and KR12C (20 μM) exhibit significant accumulation of G2/M population (10.81% to 19.83%, 17.23%, and 16.77% respectively) with a concurrent depletion in the number of the cells in G0/G1 (36.33% to 7.46%, 36.11%, and 15.26% respectively) and S (10.72% to 7.46%, 10.04%, and 8.21% respectively) phases which suggests that these peptides block cell cycle at G2/M transition. However, with increment in the peptide concentration to 40 μM, G2 phase population is declined with a concomitant increase in the population of Sub G0 phase. Similarly, for KR12B treated cells at both 20 and 40 μM, the higher number of sub G0 population probably translates into a sharp decrease in the population of all the phases.

Nuclear transport and localization of FK13 by confocal laser scanning microscopy

Confocal laser scanning microscopy is performed to observe the cellular localization of FITC labelled FK13 in MCF7 cells. MCF7 cells are treated with FITC labelled FK13 (20 μM) and incubated for 5 min to 24 hours. The cells are fixed at different time points. Fig. 5 shows the time dependent compartmentalization of the peptide, FK13 into the nuclei of MCF7 cells. These data suggest that FK13 slowly localizes to the nucleus of MCF7 cells. The merged images of DAPI and FITC labelled FK13 show nuclear localization of the peptide after 24 hour of incubation (Fig. S15†). This data suggests that FK13 is cell permeable and binds to nucleus of MCF7 cells.

The peptides (FK13, KR12A, KR12B and KR12C) down-regulates telomerase activity by Telomerase Repeat Amplification Protocol (TRAP) assay

After analysing interaction profiles of the peptides and telomeric G-quadruplex through a battery of biophysical methods, we are prompted to investigate *in vitro* the effects of the peptides on telomerase activity. We have conducted TRAP assay followed by quantitative real time PCR with the telomerase extract from telomerase overexpressed MCF7 breast cancer cells. Results demonstrate that the activity of telomerase decreases with increasing concentration of peptides (Fig. 6A). At 2.5 μM concentration of FK13, KR12A, KR12B and KR12C, the telomerase activity decreases by 4.2, 3, 1.5 and 7.1 fold respectively compared to control. Further increase in concentration of the peptides (5 μM), pronounced depletion in telomerase activity (4.2, 3, 2.3 and 9 fold respectively) is evidenced.

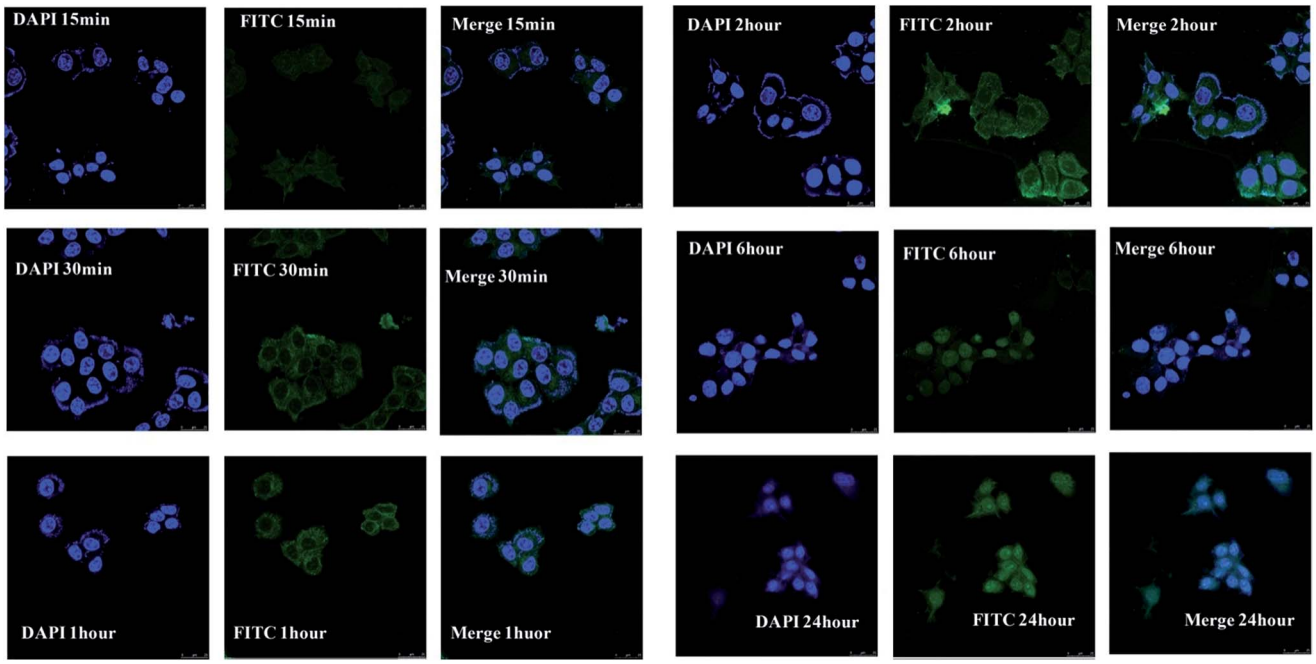

Fig. 5 Confocal microscopy images of MCF7 cell nucleus after incubation at different times. DAPI (blue) strain nucleus (left panel). FITC labeled FK13 (green) localised at nucleus of MCF7 cell (middle panel). Colocalization of DAPI and FITC-FK13 (right panel).

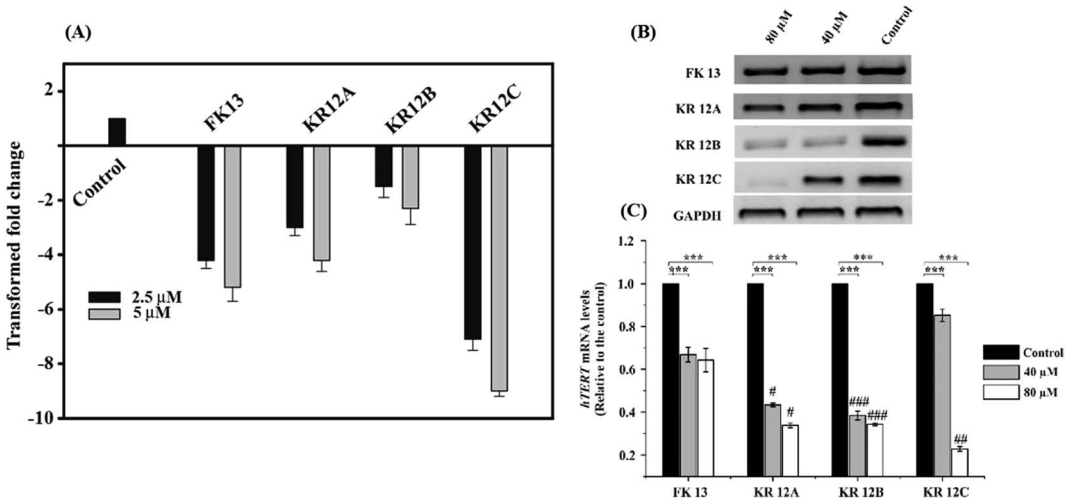

Fig. 6 (A) TRAP assay of peptides (FK13, KR12A, KR12B and KR12C) showed inhibition of the activity of enzymme, telomerase upon concentration dependent manner. (B) Depleted mRNA level of *hTERT* quantification by semi-quantitative RTPCR in peptide-treated MCF7 cell line. RTPCR was performed with specific primers for on total RNA isolated from MCF7 breast cancer cell line under the following conditions: control, 40 and 80 μM treatment with four peptides. (C) In the RTPCR analysis, the target genes were normalized to the average of internal control gene GAPDH and represented in arbitrary units. Data shown here are averaged from three independent experiments. The asterisks (*) and the hash (#) indicated statistical significance as determined from Student's *t* test (***P value < 0.001; #P value < 0.05; ##P value < 0.01; ###P value < 0.001) of the difference in mRNA profiles of cells in comparison with control and FK13 respectively.

The peptides (FK13, KR12A, KR12B, and KR12C) blocks hTERT transcription in MCF7 cells

Telomerase activity in most cancer cells is increased by the up-regulation of the expression of *hTERT* (human telomerase reverse transcriptase) gene which is the catalytic subunit of telomerase.[35] Since hTERT (human telomerase reverse transcriptase) is the catalytic subunit and the rate limiting factor in telomerase activation,[36,37] we have been speculating to find its impact upon *hTERT* expression. In this study, MCF7 cells are treated with four peptides in a concentration dependent manner. Results demonstrate that these four peptides exhibit inhibitory effect upon *hTERT* transcription (Fig. 6C and Table 4). Arresting G-quadruplex structures at human telomeric DNA, restricts the capping activity of hTERT which leads to stabilize

Table 4 Percentage of repression of hTERT mRNA expression in MCF7 cell line upon treatment with the peptides after 24 hours of incubation

Concentration	FK13	KR12A	KR12B	KR12C
Control	100	100	100	100
40 μM	36.5	37.5	58.8	18.4
80 μM	38.9	61.8	61.3	65.2

3′-single stranded overhang. RT-PCR in conjunction with TRAP assay envisage that the stable complex of peptide and telomeric G-quadruplex promotes telomere uncapping, reduces the length of single-stranded 3′-overhang (as the quadruplex is formed and stabilized) which is no longer accessed by the hTR-RNA template to elongate the 3′-end,and therefore inhibits telomerase from catalyzing telomere DNA synthesis. As a result, telomeres will succumb to progressive attrition leading to retardation of cancer cell proliferation, which we have substantiated by flow cytometry and MTT assay results. Indirectly, if telomerase is not recruited at the telomere, endogenous transcriptional repression of *hTERT* should be observed. Among the four, KR12C and KR12B exert maximal repression upon *hTERT* transcription while KR12A and FK13 engender very weak inhibition to *hTERT* expression in MCF7 cells at 40 and 80 μM concentrations.

This study show that short peptides with potential anti-cancer activity can arrest telomeric G-quadruplex structures and inhibit activity of telomerase enzyme which lead to tune back the cancer cells to natural death (apoptosis). This study enables us to develop an innovative and unique therapeutic strategy to engineer next generation peptide based agents as first in class anti-cancerous drugs.

Acknowledgements

S. C. would like to thank DST Ramanujan Fellowship and DBT grant BT/PR6627/GBD/27/440/2012. JJ, PS and SM would like to thank CSIR and CSIR-UGC for fellowships. Thanks to Mr Souvik Roy, DBT IPLS, CU for helping in ITC experiment.

References

1 R. Dahse, W. Fiedler and G. Ernst, *Clin. Chem.*, 1997, **43**, 708–714.
2 K. Paeschke, S. Juranek, T. Simonsson, A. Hempel, D. Rhodes and H. J. Lipps, *Nat. Struct. Mol. Biol.*, 2008, **15**, 598–604.
3 S. Balasubramanian, L. H. Hurley and S. Neidle, *Nat. Rev. Drug Discovery*, 2011, **10**, 261–275.
4 M. I. Zvereva, D. M. Shcherbakova and O. A. Dontsova, *Biochemistry*, 2010, **75**, 1563–1583.
5 D. Monchaud and M. P. Teulade-Fichou, *Org. Biomol. Chem.*, 2008, **6**, 627–636.
6 J. A. Schouten, S. Ladame, S. J. Mason, M. A. Cooper and S. Balasubramanian, *J. Am. Chem. Soc.*, 2003, **125**, 5594–5595.
7 B. Heddi, V. V. Cheong, H. Martadinata and A. T. Phan, *Proc. Natl. Acad. Sci. U. S. A.*, 2015, **112**, 9608–9613.
8 H. M. Chen, W. Wang, D. Smith and S. C. Chan, *Biochim. Biophys. Acta*, 1997, **1336**, 171–179.
9 D. W. Hoskin and A. Ramamoorthy, *Biochim. Biophys. Acta*, 2008, **1778**, 357–375.
10 K. Matsuzaki, K. Sugishita, M. Harada, N. Fujii and K. Miyajima, *Biochim. Biophys. Acta*, 1997, **1327**, 119–130.
11 M. Zasloff, *Nature*, 2002, **415**, 389–395.
12 H. Schröder-Borm, R. Bakalova and J. Andrä, *FEBS Lett.*, 2005, **579**, 6128–6134.
13 J. Johansson, G. H. Gudmundsson, M. E. Rottenberg, K. D. Berndt and B. Agerberth, *J. Biol. Chem.*, 1998, **273**, 3718–3724.
14 W. K. Wu, G. Wang, S. B. Coffelt, A. M. Betancourt, C. W. Lee, D. Fan, K. Wu, J. Yu, J. J. Sung and C. H. Cho, *Int. J. Cancer*, 2010, **127**, 1741–1747.
15 U. H. Dürr, U. S. Sudheendra and A. Ramamoorthy, *Biochim. Biophys. Acta*, 2006, **1758**, 1408–1425.
16 J. Jana, R. K. Kar, A. Ghosh, A. Biswas, S. Ghosh, A. Bhunia and S. Chatterjee, *Mol. BioSyst.*, 2013, **9**, 1833–1836.
17 D. A. Case, T. E. Cheatham, T. Darden, H. Gohlke, R. Luo, K. M. Merz, A. Onufriev, C. Simmerling, B. Wang and R. J. Woods, *J. Comput. Chem.*, 2005, **26**, 1668–1688.
18 A. Pérez, I. Marchán, D. Svozil, J. Sponer, T. E. Cheatham, C. A. Laughton and M. Orozco, *Biophys. J.*, 2007, **92**, 3817–3829.
19 W. Jorgensen, J. Chandrasekhar, J. D. Madura, R. W. Impey and M. L. Klein, *J. Chem. Phys.*, 1983, **79**, 926–935.
20 Y. Shan, J. L. Klepeis, M. P. Eastwood, R. O. Dror and D. E. Shaw, *J. Chem. Phys.*, 2005, **122**, 54101.
21 V. Krutler, W. F. V. Gunsteren and P. H. Hunenberger, *J. Comput. Chem.*, 2001, **22**, 501–508.
22 D. Roe and T. E. Cheatham, *J. Chem. Theory Comput.*, 2013, **9**, 3084–3095.
23 S. Mondal, J. Jana, P. Sengupta, S. Jana and S. Chatterjee, *Mol. BioSyst.*, 2016, **12**, 2506–2518.
24 X. Li, Y. Li, H. Han, D. W. Miller and G. Wang, *J. Am. Chem. Soc.*, 2006, **128**, 5776–5785.
25 G. Wang, *J. Biol. Chem.*, 2008, **283**, 32637–32643.
26 B. Jacob, I. S. Park, J. K. Bang and S. Y. Shin, *J. Pept. Sci.*, 2013, **19**, 700–707.
27 K. V. Reddy, R. D. Yedery and C. Aranha, *Int. J. Antimicrob. Agents*, 2004, **24**, 536–547.
28 J. Kypr, I. Kejnovská, D. Renciuk and M. Vorlícková, *Nucleic Acids Res.*, 2009, **37**, 1713–1725.
29 J. S. Mader and D. W. Hoskin, *Expert Opin. Invest. Drugs*, 2006, **15**, 933–946.
30 L. Yu, M. Tan, B. Ho, J. L. Ding and T. Wohland, *Anal. Chim. Acta*, 2006, **556**, 216–225.
31 A. Bhunia, R. Saravanan, H. Mohanram, M. L. Mangoni and S. Bhattacharjya, *J. Biol. Chem.*, 2011, **286**, 24394–24406.
32 A. T. Phan, V. Kuryavyi, K. N. Luu and D. J. Patel, *Nucleic Acids Res.*, 2007, **35**, 6517–6525.
33 T. Kanaya, S. Kyo, M. Takakura, H. Ito, M. Namiki and M. Inoue, *Int. J. Cancer*, 1998, **78**, 539–543.

34 C. Ramachandran, H. B. Fonseca, P. Jhabvala, E. A. Escalon and S. J. Melnick, *Cancer Lett.*, 2002, **184**, 1–6.
35 V. Sekaran, J. Soares and M. B. Jarstfer, *J. Med. Chem.*, 2014, **57**, 521–538.
36 M. Ruden and N. Puri, *Cancer Treat. Rev.*, 2013, **39**, 444–456.
37 F. Pendino, I. Tarkanyi, C. Dudognon, J. Hillion, M. Lanotte, J. Aradi and E. Ségal-Bendirdjian, *Curr. Cancer Drug Targets*, 2006, **6**, 147–180.